

---

This is an electronic reprint of the original article.  
This reprint may differ from the original in pagination and typographic detail.

Najafi Jabdaraghi, Robab; Peltonen, Joonas; Saira, Olli-Pentti; Pekola, Jukka  
**Low-temperature characterization of Nb-Cu-Nb weak links with Ar ion-cleaned interfaces**

*Published in:*  
Applied Physics Letters

*DOI:*  
[10.1063/1.4940979](https://doi.org/10.1063/1.4940979)

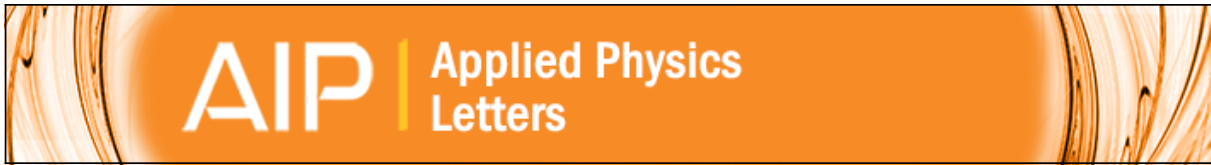
Published: 25/01/2016

*Document Version*  
Publisher's PDF, also known as Version of record

*Please cite the original version:*  
Najafi Jabdaraghi, R., Peltonen, J., Saira, O.-P., & Pekola, J. (2016). Low-temperature characterization of Nb-Cu-Nb weak links with Ar ion-cleaned interfaces. *Applied Physics Letters*, 108(4), 1-5. Article 042604.  
<https://doi.org/10.1063/1.4940979>

---

This material is protected by copyright and other intellectual property rights, and duplication or sale of all or part of any of the repository collections is not permitted, except that material may be duplicated by you for your research use or educational purposes in electronic or print form. You must obtain permission for any other use. Electronic or print copies may not be offered, whether for sale or otherwise to anyone who is not an authorised user.



## Low-temperature characterization of Nb-Cu-Nb weak links with Ar ion-cleaned interfaces

R. N. Jabdaraghi, J. T. Peltonen, O.-P. Saira, and J. P. Pekola

Citation: [Applied Physics Letters](#) **108**, 042604 (2016); doi: 10.1063/1.4940979

View online: <http://dx.doi.org/10.1063/1.4940979>

View Table of Contents: <http://scitation.aip.org/content/aip/journal/apl/108/4?ver=pdfcov>

Published by the [AIP Publishing](#)

---

### Articles you may be interested in

[Micro-superconducting quantum interference devices based on V/Cu/V Josephson nanojunctions](#)

*Appl. Phys. Lett.* **103**, 052603 (2013); 10.1063/1.4817013

[Controllable Josephson current through a pseudospin-valve structure](#)

*Appl. Phys. Lett.* **84**, 1153 (2004); 10.1063/1.1646217

[Harmonic current-phase relation in Nb–Al-based superconductor/insulator/normal conductor/insulator/superconductor-type Josephson junctions between 4.2 K and the critical temperature](#)

*Appl. Phys. Lett.* **77**, 1354 (2000); 10.1063/1.1290142

[Direct writing of low  \$T\_c\$  superconductor-normal metal-superconductor junctions using a focused ion beam](#)

*Appl. Phys. Lett.* **75**, 262 (1999); 10.1063/1.124342

[Anomalous critical current in double-barrier Nb/Al–AlO<sub>x</sub> – Al–AlO<sub>x</sub> – Nb devices](#)

*Appl. Phys. Lett.* **74**, 1624 (1999); 10.1063/1.123637

---

The image shows the cover of an Applied Physics Reviews journal issue. It features a blue and orange color scheme with a molecular structure background. The text 'NEW Special Topic Sections' is prominently displayed in white. Below it, 'NOW ONLINE' is written in yellow, followed by the title 'Lithium Niobate Properties and Applications: Reviews of Emerging Trends' in white. The AIP Applied Physics Reviews logo is in the bottom right corner.

**NEW Special Topic Sections**

**NOW ONLINE**  
Lithium Niobate Properties and Applications:  
Reviews of Emerging Trends

**AIP** Applied Physics  
Reviews

## Low-temperature characterization of Nb-Cu-Nb weak links with Ar ion-cleaned interfaces

R. N. Jabdaraghi,<sup>1,2,a)</sup> J. T. Peltonen,<sup>1</sup> O.-P. Saira,<sup>1</sup> and J. P. Pekola<sup>1</sup>

<sup>1</sup>Low Temperature Laboratory, Department of Applied Physics, Aalto University School of Science, P.O. Box 13500, FI-00076 Aalto, Finland

<sup>2</sup>Faculty of Physics, University of Tabriz, 51665-163 Tabriz, Iran

(Received 13 October 2015; accepted 16 January 2016; published online 27 January 2016)

We characterize niobium-based lateral Superconductor (S)–Normal metal (N)–Superconductor (SNS) weak links through low-temperature switching current measurements and tunnel spectroscopy. We fabricate the SNS devices in two separate lithography and deposition steps, combined with strong argon ion cleaning before the normal metal deposition in the last step. Our SNS weak link consists of high-quality sputtered Nb electrodes that have contacted with evaporated Cu. The two-step fabrication flow enables more flexibility in the choice of materials and pattern design. A comparison of the temperature-dependent equilibrium critical supercurrent with theoretical predictions indicates that the quality of the Nb-Cu interface is similar to that of evaporated Al-Cu weak links. We further demonstrate a hybrid magnetic flux sensor based on an Nb-Cu-Nb SNS junction, where the phase-dependent normal metal density of states is probed with an Al tunnel junction.

© 2016 AIP Publishing LLC. [<http://dx.doi.org/10.1063/1.4940979>]

A Superconductor–Normal metal–Superconductor (SNS) weak link<sup>1–4</sup> consists of a short normal conducting metal (N) embedded between two superconducting (S) electrodes and supports supercurrent due to the proximity effect.<sup>2,5–11</sup> Lateral SNS weak links allow the creation of further novel types of interferometers<sup>12,13</sup> with a large number of foreseen applications, including measurement of magnetic flux induced by atomic spins, single-photon detection, and nanoelectrical measurements.<sup>14–16</sup> In many instances, the performance of these sensors improves when the proximity effect in the N wire, as measured by the magnitude of the induced (mini)gap, is maximized. In this respect, moving to a large-gap superconductor such as Nb or Nb(Ti)N is an evident direction to look for performance gains.

Aluminium-based weak links with well controlled interface transparencies are routinely fabricated by shadow evaporation through a bilayer mask<sup>17</sup> that allows deposition of the superconducting and normal electrodes in a single vacuum cycle. When it comes to superconductors with higher  $T_c$  compared to Al, vanadium is one of the few that are easily suited for shadow evaporation.<sup>18,19</sup> On the other hand, in Ref. 20, the critical currents in shadow-evaporated Nb-Cu-Nb SNS junctions, measured down to 300 mK, were found to be in excellent agreement with theoretical predictions. However, the evaporation of good quality Nb films requires significant attention due to the high melting temperature and the resulting organic resist outgassing: Either a bilayer mask with a special thermostable polymer,<sup>21,22</sup> a fully inorganic mask,<sup>23,24</sup> or an evaporator with large target-to-sample distance<sup>25</sup> has to be used.

For many detector applications of SNS weak links such as sensitive hot-electron bolometers and calorimeters,<sup>26,27</sup> it can be moreover desirable to avoid any unwanted normal metal structures, including the shadow replicas always

present after multi-angle evaporation. An etching-based, two-step process would also be preferable on the grounds of unrestricted geometry when combining proximity weak links with high-quality superconducting resonators patterned from Nb, Ta, or other difficult-to-evaporate materials. In addition, if such Nb structures are to be combined with shadow evaporated structures and tunnel junctions, it is advantageous to start with the Nb deposition: The tunnel junctions or merely individual thin films of several materials are likely to show degradation if they are not formed in the last process step. An alternative approach would be to start by fabricating the normal metal electrode from a noble metal, e.g., gold, whose surface is relatively easy to clean, and to deposit the Nb electrode only in the second step. However, due to added complexity, this may not be optimal in combining such an SNS weak link with shadow evaporated tunnel probes in further steps.

In this letter, we present a study of sputtered niobium-based SNS weak links where the normal metal electrode is deposited shortly after an *in situ* argon ion etching. Similar junctions with Ar-cleaned interfaces have been fabricated before,<sup>20,28–30</sup> but a detailed investigation in a simple SNS geometry has not been reported. We further present an experimental demonstration of an Nb-based SQUIPT (superconducting quantum interference proximity transistor) interferometer.<sup>13</sup> In an initial device, we observe maximum flux-to-current transfer function values of about  $|\partial I/\partial \Phi|_{\max} = 50 \text{ nA}/\Phi_0$  at  $T = 80 \text{ mK}$ . Here,  $\Phi_0 = h/(2e)$  is the superconducting flux quantum. The S–N interface quality of the devices is verified by comparing the temperature dependence of the measured critical (switching) current with a theoretical model valid in the diffusive limit. We consider both triangular and rectangular shaped S electrode terminations (see Fig. 1, insets), referred to as geometry A and B, respectively. The thickness profile at the tip of the electrode is more gentle for geometry A, which may affect the contact quality and the extent of inverse proximity effect.

<sup>a)</sup>Electronic mail: [robab.najafi.jabdaraghi@aalto.fi](mailto:robab.najafi.jabdaraghi@aalto.fi)

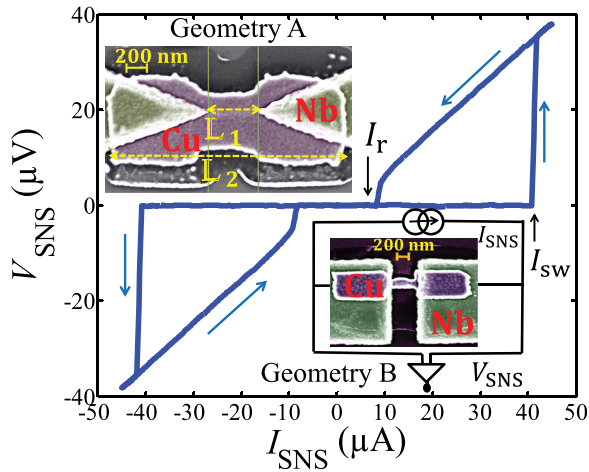


FIG. 1. Main panel: current–voltage characteristic of sample B2 measured at  $T = 80$  mK. Arrows indicate the switching  $I_{sw}$  and retrapping current  $I_r$ . The top (bottom) inset shows a representative scanning electron micrograph of a junction with geometry A (B), consisting of a normal metal (Cu) island embedded between two superconducting electrodes (Nb). The distance between the superconducting electrodes is  $L_1$ , whereas  $L_2$  is the total N length. The bottom inset includes a sketch of the measurement setup.

Minimized S electrode separation with good fabrication yield is needed for optimal sensitivity in sensor applications. We specifically focus on combining the Ar-cleaned Nb structures with shadow-evaporated normal and superconducting metals.

The fabrication process consists of two main steps: First making the Nb structures and then providing clean electric contact between Nb and Cu. The starting point is an oxidized 4 in. Si substrate with 200 nm sputter-deposited Nb. An etch mask based on positive tone AR-P 6200.13 resist is prepared by electron-beam lithography (EBL), followed by wet development and 5 min reflow baking at 150 °C to avoid abrupt edge profiles in the Nb structures. Reactive ion etching (RIE) with a mixture of SF<sub>6</sub> and Ar is then used to transfer the pattern into the Nb film. We employed gas flows of 20 sccm and 10 sccm for SF<sub>6</sub> and Ar, respectively, and the 100 W RF power resulted typically in DC self-bias of 300 – 320 V. Nb etching is followed by a second round of EBL using a conventional bilayer resist.<sup>17</sup> In our case, this consists of a 200 nm (600 nm) thick poly(methyl methacrylate) layer for geometry A (B), on top of a 900 nm layer of copolymer.

The crucial step in the fabrication is to create a transparent contact between Nb and Cu. This is done by exposing the chip to *in situ* Ar ion etching, in the same vacuum cycle immediately prior to the Cu deposition. Based on profilometer traces, we estimate that typically 10 – 20 nm of Nb is removed in this cleaning step. To complete the SNS junction, the 60 nm thick normal metal Cu electrode is deposited by electron-gun evaporation. We find typical low-temperature values of the Cu sheet resistance  $R_{\square}$  to be in the range of 0.4 – 0.5 Ω. The Ar ion flux is meeting the sample perpendicular to the substrate, same as the deposited Cu.

The main panel of Fig. 1 shows the current–voltage characteristic of one of the measured samples, SNS junction B2, featuring a well-defined supercurrent. All the measurements were performed in a dilution refrigerator, down to the base temperature between 50 and 100 mK. As indicated in the bottom inset of Fig. 1, the weak link is biased by a

current  $I_{SNS}$  and the dc voltage  $V_{SNS}$  is measured in a four-probe configuration. In this sample, we observe hysteretic behavior at  $T < 0.65$  K, originating mainly from self-heating in the finite-voltage state.<sup>21,31,32</sup> At  $T < 100$  mK, we deduce a switching current  $I_{sw}$  and retrapping current  $I_r$  of about 42 μA and 9 μA, respectively.

The parameters of the measured junctions are listed in Table I. The symbols in Fig. 2 summarize the measured switching currents  $I_{sw}$  as a function of the bath temperature  $T$  for four of the samples. For clarity, the inset in Fig. 2 further shows the temperature dependence of the switching and retrapping currents for sample B2 on a linear scale. We find no qualitative differences in the behavior of the switching currents between junction geometries A and B.

In diffusive metallic SNS junctions, the natural energy scale for the proximity effect is given by the Thouless energy  $E_{Th} = \hbar D/L^2$ , where  $D$  and  $L$  are the diffusion coefficient and the length of the normal metal electrode, respectively. Our samples are in the long junction limit  $L \gg \xi_0$ , or equivalently  $\Delta \gg E_{Th}$ , where  $\xi_0 = (\hbar D/\Delta)^{1/2}$  and  $\Delta \approx 1.2$  meV denote the superconducting coherence length and energy gap, respectively. The solid lines in Fig. 2 are calculated according to

$$I_{sw} = \frac{\alpha E_{Th}}{2eR_N} \int_{-\infty}^{\infty} dE \operatorname{Im}[j_E(E)] \tanh\left(\frac{E}{2k_B T}\right). \quad (1)$$

Here, the energy-dependent quantity  $j_E(E)$ , depending only weakly on the ratio  $\Delta/E_{Th}$  in the long junction limit, is a spectral supercurrent obtained from a numerical solution of the Usadel equations in a 1D SNS geometry, assuming perfectly transparent interfaces.<sup>20,33</sup> For the samples in Fig. 2, at  $T > 0.2$  K, Eq. (1) practically coincides with its high-temperature analytical approximation<sup>34</sup> valid at  $k_B T \gg E_{Th}$  [see Eq. (1) in Ref. 20]. In the model, we neglected the self-consistency and temperature dependence of the order parameter, as well as assumed a sinusoidal current-phase relation.<sup>10,33</sup>

As adjustable parameters we use the Thouless energy  $E_{Th}$  and a dimensionless reduction parameter  $\alpha$ . The values resulting in best agreement are listed in Table I for all

TABLE I. Parameters of measured samples.  $L_1$  is the minimum Nb electrode separation in the SNS junction,  $L_2$  the full length of Cu wire, and  $w$  the minimum width of the copper island (see Fig. 1).  $E_{Th}$  (and hence  $L$ ) and  $\alpha$  are obtained from a comparison of the temperature-dependent switching current measurements to the theoretical model.  $R_N$  is the measured low-temperature normal state resistance of the wire, and  $I_{sw}^{\max}$  denotes the maximum observed switching current.

Sample	$L_1$ (μm)	$L_2$ (μm)	$w$ (μm)	$L$ (μm)	$\alpha$	$R_N$ (Ω)	$E_{Th}$ (μeV)	$I_{sw}^{\max}$ (μA)	$\frac{eR_N I_{sw}^{\max}}{E_{Th}}$
A1	0.29	2	0.55	1.09	0.52	0.83	5.5	33	5
A2	0.36	2	0.55	1.18	0.67	0.83	4.7	33	5.9
A3	0.48	2.15	0.54	1.18	0.48	0.57	4.8	30	3.6
A4	0.49	2.15	0.54	1.21	0.5	0.59	4.5	30	4
A5	0.84	2.5	0.85	1.80	0.49	0.5	2	10	2.5
B1	0.32	2	0.15	1.09	0.61	0.98	7.7	42	5.3
B2	0.38	2	0.15	1.09	0.57	0.89	7.3	41	5
B3	0.40	2.12	0.15	0.96	0.5	2.31	7	14	4.6
B4	0.39	2.17	0.14	0.91	0.47	2.42	8	14	4.3
B5	0.40	2.12	0.15	0.85	0.53	2.51	9	18	5

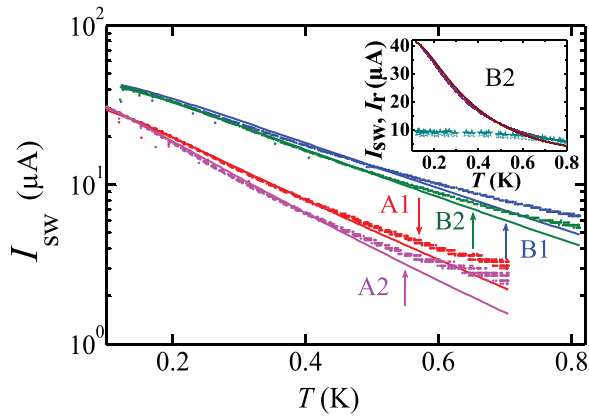


FIG. 2. The symbols show the temperature dependence of the measured  $I_{sw}$  of samples A1, A2, B1, and B2. The solid lines show predictions of a simple model based on the Usadel equations [Eq. (1)]. The adjustable parameters are the Thouless energy  $E_{Th}$  and reduction parameter  $\alpha$ . The vertical arrows identify the samples and indicate the temperature below which the hysteresis in the IV curve appears for each of them. Inset: Temperature dependence of the measured  $I_{sw}$  together with the theoretical model (solid lines) for sample B2. The star symbols show the retrapping current  $I_r$ , which is almost temperature-independent in the hysteretic regime.

samples. The effective junction lengths  $L$ , derived from the estimated values of  $E_{Th}$  and the measured Cu diffusion constant  $D \approx 0.01 \text{ m}^2 \text{ s}^{-1}$ , satisfy  $L_1 < L < L_2$  as expected. Depending on the sample geometry, we obtain values for the effective lengths  $L/\xi_0 \approx 15 - 20$ , corresponding to  $\Delta/E_{Th} \approx 130 - 600$ . The values of  $L$  are larger than  $L_1$  but smaller than  $L_2$  due to the inverse proximity effect where the Cu island overlaps the Nb electrodes.

In a first approximation, the overlap areas can be modeled as superconductors with a reduced coupling factor, suppressed by the ratio of the S thickness to the total bilayer thickness. Exact modeling of the true overlap geometry of our NS contacts in terms of the 1D Usadel equations is, however, not straightforward: In the present devices, both the Cu wire width and the Nb electrode thickness (and width for geometry A) are varying along the weak link. An accurate estimate of the effective length requires a self-consistent simulation. Therefore, we have performed the fit using the 1D model for a basic junction with an effective length. For comparison, in Ref. 20 with fully shadow-evaporated Nb-Cu junctions, a good agreement to theory was found using the full length of the N wire, giving  $L \approx L_1 + 300$  to 400 nm. Minimizing  $L$  is important for sensor applications of the structures fabricated using the two-step method. Besides further reducing  $L_1$ , we intend to make future experiments with N wires of constant cross section and different lengths of the overlap region.

Observed values of  $\alpha < 1$  and  $L > L_1$  can account for partially transparent interfaces.<sup>33,35</sup> However, based on the measured values of  $R_N \approx R_L + 2R_1$  and separate estimation of the Cu wire resistances, we find all the studied samples to clearly satisfy the condition  $R_L < R_1$ . Here,  $R_L$  is the N island resistance and  $2R_1$  the total resistance of the contacts. The transparent nature of the contacts is further supported by separate room-temperature resistance measurements of Nb/Cu reference structures, and indirectly by the fact that we find  $\alpha \approx 0.5$  for our shadow-evaporated Al-Cu weak links measured in the same setup.<sup>32</sup> Several other factors can also

contribute to suppression of the observed  $I_{sw}$  below the true critical current  $I_c$ . First, for SNS junctions with intrinsically overdamped phase dynamics, but exhibiting thermal hysteresis due to self-heating, the observed switching can be slightly below  $I_c$  due to local heating by phase diffusion, cf. Ref. 32. Second, the nominally overdamped junctions can show intrinsic hysteresis due to an effective capacitance  $C_{eff} = \tau_D/R_N$ . Here,  $\tau_D = \hbar/E_{Th}$  is the diffusion time in the normal wire.<sup>36</sup> We estimate that for our junctions this can lead to typically at most 5%–10% suppression of  $I_{sw}$  below  $I_c$ . The combined effect of the various causes for  $I_{sw}$  suppression in SNS junctions is difficult to quantify, and it is the subject of our on-going measurements.

The model with a single temperature-independent  $L$  and  $\alpha$  is not able to capture the behavior of the critical current at the highest temperatures. A part of the deviation is explained by the measurement accuracy and the uncertainty in extracting  $I_{sw}$  from the measured IV characteristics: In the hysteretic, low-temperature regime with a clear jump in  $V_{SNS}$  at  $I_{sw}$ , the switching current is extracted to an accuracy within  $\delta I$ , the step size of the bias current  $I_{SNS}$ . For the measurements in Fig. 2, the coarse values  $0.3 \mu\text{A}$  for samples A1 and A2 and  $0.2 \mu\text{A}$  for samples B1 and B2 were used. In the non-hysteretic regime, the uncertainty for determining  $I_{sw}$  is larger, at least  $2\delta I$  at the highest temperatures in Fig. 2. Further detailed measurements optimized for the non-hysteretic region are needed to draw reliable conclusions about the high-temperature behavior of  $I_{sw}$  in these structures.

In samples A5 and B3–B5, the normal metal Cu electrode was deposited immediately after the Ar cleaning. With the rest of the samples, we investigated combining the Nb-Cu-Nb weak link with an Al-AlOx-Cu Normal metal–Insulator–Superconductor (NIS) tunnel junction. To this end, structures A1–A4 and B1–B2 were fabricated simultaneously with SQUIPT-interferometers (see the following paragraphs and Fig. 3) located elsewhere on the same chip. In these SNS junctions, after Ar cleaning but prior to Cu deposition, the Nb contact areas were controllably exposed to an atmosphere of pure oxygen, typically for 1–5 min at a pressure of 1–5 mbar. Importantly, based on values of  $R_N$ ,  $L$ , and  $\alpha$ , we conclude that this *in situ* oxidation of the exposed Nb contact surfaces has less influence on the SNS weak link properties than variation between different fabrication rounds in the alignment of the Cu island, the Cu deposition, and the nominally identical Ar etching conditions.

We now consider an application of the fabrication technique described above. Imposing a phase difference between the superconducting electrodes of a SNS junction provides a means to modulate the density of states (DoS) in the N electrode and the supercurrent through the weak link.<sup>12,37,38</sup> A SQUIPT interferometer,<sup>13</sup> see Fig. 3(a), consists of an SNS link embedded into a superconducting loop. When placed into perpendicular magnetic field, the flux-dependent density of states can be accurately probed with a weakly coupled tunnel junction in contact with the N electrode. The performance of such hybrid devices with Al-Cu weak links has improved as a result of several studies.<sup>13,39–42</sup> To realize an Nb-SQUIPT with our present technique, we first prepare a suitable shadow mask and Ar etch the Nb contacts, in a

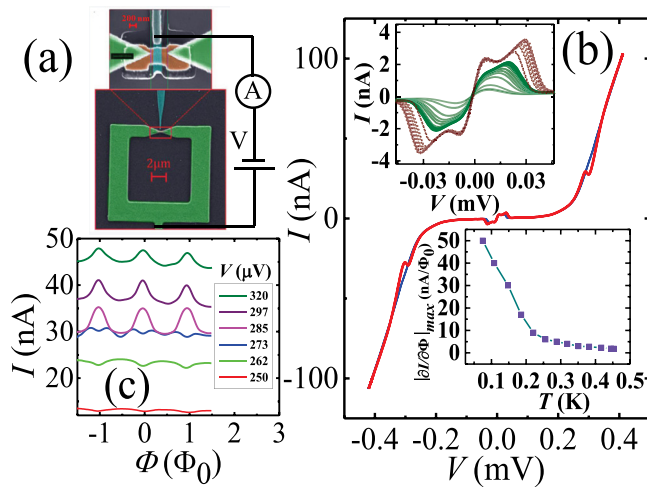


FIG. 3. (a) False color scanning electron micrograph of an initial Nb-SQUIPT, together with the scheme for measurement under voltage bias. The enlarged view emphasizes the Al superconducting tunnel probe (cyan) connected to the middle of the Cu island (brown) in the Nb-Cu-Nb weak link. Nb electrodes and the loop are shown in green. (b) IV characteristics of a Nb-SQUIPT based on an A-type SNS junction measured at  $T = 80$  mK, for two values of magnetic flux through the loop:  $\Phi = 0$  (red) and  $\Phi = 0.5\Phi_0$  (blue). The upper inset shows the flux modulation of the IV curve around zero bias voltage at  $T = 190$  mK (green solid) and  $T = 80$  mK (brown dashed lines) while the lower inset presents temperature dependence of the maximum flux-to-current transfer function  $|\partial I/\partial\Phi|_{\max}$  on the supercurrent branch. (c) Current modulation  $I(\Phi)$  at  $T = 80$  mK for several values of the bias voltage between 250 (bottom curve, red) and 320  $\mu\text{V}$  (top curve, dark green).

fashion identical to the Nb-Cu-Nb weak links above. Then, without breaking the vacuum, immediately before the Cu evaporation, a 20 nm thick Al electrode of the NIS junction is deposited and subjected to *in situ* oxidation to create the thin AlOx tunnel barrier.

Figure 3(b) displays the IV characteristics of the device measured at two different magnetic fields,  $\Phi = 0$  and  $\Phi = 0.5\Phi_0$ , corresponding to maximum and minimum minigap opened in the normal metal.<sup>10,43</sup> We observe a flux-dependent onset of current on the quasiparticle branch when  $|V|$  exceeds the sum of the probe electrode gap  $\Delta_{\text{Al}}/e$  and the minigap induced in the N wire. At  $T = 80$  mK, we further find a maximum supercurrent of 3.6 nA, evident as the flux-dependent peak close to zero voltage bias. Due to the larger junction size and the relatively low tunnel resistance  $R_T \approx 3$  k $\Omega$ , this feature is pronounced compared to earlier experiments.<sup>13,40,41</sup> The solid green lines in the upper inset of Fig. 3(b) demonstrate the extent of the flux modulation of the IV curve around zero bias at  $T = 190$  mK, where we observe almost full phase modulation due to increased SNS weak link inductance compared to the Nb loop inductance.<sup>41</sup> For comparison, the IVs at  $T = 80$  mK are included as the dashed brown lines.

To characterize the flux sensitivity of the SQUIPT device, we measured  $I(\Phi)$  curves at several values of the constant bias voltage  $V$  and subsequently obtained the flux-to-current transfer function  $\partial I/\partial\Phi$  by numerical differentiation. Figure 3(c) shows some of the flux modulations  $I(\Phi)$  measured at  $V$  around the onset of the quasiparticle current. In this range of bias voltages, we find the maximum sensitivity  $|\partial I/\partial\Phi|_{\max} \approx 40$  nA/ $\Phi_0$ . Interestingly, for this device, the overall maximum  $|\partial I/\partial\Phi|_{\max} \approx 50$  nA/ $\Phi_0$ , at the base

temperature around 80 mK, is reached in the supercurrent branch at  $V \approx 32$   $\mu\text{V}$ . For comparison,  $|\partial I/\partial\Phi|_{\max} \approx 100$  nA/ $\Phi_0$  at  $T = 240$  mK has been recently reported for an optimized Al-SQUIPT.<sup>41</sup> The temperature dependence of the maximum sensitivity in the low-bias regime is further shown in the bottom inset of Fig. 3(b), decreasing monotonously as  $T$  increases. We note that the Al tunnel junction can be straightforwardly replaced by a normal-conducting probe for zero-bias operation with reduced dissipation.<sup>44</sup>

Advantages of devices fabricated using our two-step process include a larger range of operation temperatures and better thermal isolation due to the larger  $\Delta$  of the S leads. Furthermore, the device geometry is not restricted by limitations of the shadow mask technique. This allows, for example, separate optimization of the SQUIPT interferometer loop, or straightforward integration of the SNS weak link with a high-quality superconducting resonator, e.g., in calorimeter applications.<sup>26,27</sup> The most significant improvements to the performance of the initial realization of a Nb-SQUIPT are expected to result from decreasing the effective length  $L$  of the SNS weak link closer to the intermediate-to-short junction regime. We estimate that the present etching and lithography techniques allow  $L_1$  to be reliably reduced down to slightly below 100 nm in both studied lead geometries, in particular, with somewhat thinner Nb electrodes. For consistent values of  $L_1$ , the rectangular geometry is preferable. Together with shorter Nb-Cu overlap lengths, i.e.,  $L_2$  closer to  $L_1$ , this would bring the theoretical performance estimates for an Nb-SQUIPT with  $L = 150$  nm within reach: For optimized parameters, transfer functions up to a few mV/ $\Phi_0$  under current bias and intrinsic flux noise in the  $10^{-9}\Phi_0/\sqrt{\text{Hz}}$  range have been predicted.<sup>13,42</sup> The sensitivity may further increase with narrower Al probe junctions, leading to less spatial averaging of the N DoS, as a result of optimization of the Ar cleaning step and the shadow mask. In the present device, we observe a notable broadening of the geometry after the *in situ* etching.

In conclusion, we have investigated Nb-Cu-Nb weak links based on two independent lithography and deposition steps, relying on Ar ion cleaning of the Nb contact surfaces. The work helps in improving the performance of superconducting magnetometers, as well as in including submicron lateral SNS weak links in other detector applications, such as ultrasensitive bolometers and calorimeters, where they need to be integrated with shadow-evaporated tunnel junctions.

The work has been supported by the Academy of Finland Centre of Excellence program (Project No. 250280). We acknowledge the Iranian Ministry of Science, Research and Technology, Micronova Nanofabrication Centre of Aalto University for providing the processing facilities, and VTT Technical Research Centre of Finland for the sputtered Nb films. We thank D. Golubev, M. Meschke, and P. Virtanen for helpful discussions.

<sup>1</sup>K. Likharev, *Dynamics of Josephson Junctions and Circuits* (Gordon and Breach Sciences Publishers, 1991).

<sup>2</sup>M. Tinkham, *Introduction to Superconductivity*, 2nd ed. (McGraw-Hill, New York, 1996).

<sup>3</sup>J. Clarke, *Proc. R. Soc. London* **308**, 447 (1969).

<sup>4</sup>J. Clarke, *Phys. Rev. B* **4**, 2963 (1971).

- <sup>5</sup>P. G. de Gennes, *Superconductivity of Metals and Alloys* (W. A. Benjamin, New York, 1966).
- <sup>6</sup>P. G. de Gennes, *Rev. Mod. Phys.* **36**, 225 (1964).
- <sup>7</sup>A. I. Buzdin, *Rev. Mod. Phys.* **77**, 935 (2005).
- <sup>8</sup>W. Belzig, F. K. Wilhelm, C. Bruder, G. Schön, and A. D. Zaikin, *Superlattices Microstruct.* **25**, 1251 (1999).
- <sup>9</sup>B. Pannetier and H. Courtois, *J. Low Temp. Phys.* **118**, 599 (2000).
- <sup>10</sup>H. le Sueur, P. Joyez, H. Pothier, C. Urbina, and D. Esteve, *Phys. Rev. Lett.* **100**, 197002 (2008).
- <sup>11</sup>D. Roditchev, C. Brun, L. Serrier-Garcia, J. C. Cuevas, V. H. L. Bessa, M. V. Milosevic, F. Debontridder, V. Stolyarov, and T. Cren, *Nat. Phys.* **11**, 332 (2015).
- <sup>12</sup>V. T. Petrashov, V. N. Antonov, P. Delsing, and T. Claeson, *Phys. Rev. Lett.* **74**, 5268 (1995).
- <sup>13</sup>F. Giazotto, J. T. Peltonen, M. Meschke, and J. P. Pekola, *Nat. Phys.* **6**, 254 (2010).
- <sup>14</sup>C. P. Foley and H. Hilgenkamp, *Supercond. Sci. Technol.* **22**, 064001 (2009).
- <sup>15</sup>L. Hao, J. C. Macfarlane, S. K. H. Lam, C. P. Foley, P. Josephs-Franks, and J. C. Gallop, *IEEE Trans. Appl. Supercond.* **15**, 514 (2005).
- <sup>16</sup>L. Hao, J. C. Macfarlane, J. C. Gallop, D. Cox, P. Joseph-Franks, D. Hutson, and J. Chen, *IEEE Trans. Instrum. Meas.* **56**, 392 (2007).
- <sup>17</sup>G. J. Dolan, *Appl. Phys. Lett.* **31**, 337 (1977).
- <sup>18</sup>C. P. Garcia and F. Giazotto, *Appl. Phys. Lett.* **94**, 132508 (2009).
- <sup>19</sup>A. Ronzani, M. Baillergeau, C. Altimiras, and F. Giazotto, *Appl. Phys. Lett.* **103**, 052603 (2013).
- <sup>20</sup>P. Dubos, H. Courtois, B. Pannetier, F. K. Wilhelm, A. D. Zaikin, and G. Schön, *Phys. Rev. B* **63**, 64502 (2001).
- <sup>21</sup>F. Chiodi, M. Aprili, and B. Reulet, *Phys. Rev. Lett.* **103**, 177002 (2009).
- <sup>22</sup>P. Dubos, P. Charlat, Th. Crozes, P. Paniez, and B. Pannetier, *J. Vac. Sci. Technol. B* **18**, 122 (2000).
- <sup>23</sup>T. Hoss, C. Strunk, and C. Schönenberger, *Microelectron. Eng.* **46**, 149 (1999).
- <sup>24</sup>S. Samaddar, D. van Zanten, A. Fay, B. Sacépé, H. Courtois, and C. B. Winkelmann, *Nanotechnology* **24**, 375304 (2013).
- <sup>25</sup>N. Kim, K. Hansen, J. Toppari, T. Suppala, and J. Pekola, *J. Vac. Sci. Technol. B* **20**, 386 (2002).
- <sup>26</sup>J. Govenius, R. E. Lake, K. Y. Tan, V. Pietilä, J. K. Julin, I. J. Maasilta, P. Virtanen, and M. Möttönen, *Phys. Rev. B* **90**, 064505 (2014).
- <sup>27</sup>S. Gasparinetti, K. L. Viisanen, O.-P. Saira, T. Faivre, M. Arzeo, M. Meschke, and J. P. Pekola, *Phys. Rev. Appl.* **3**, 014007 (2015).
- <sup>28</sup>J. J. A. Baselmans, B. J. van Wees, and T. M. Klapwijk, *Appl. Phys. Lett.* **79**, 2940 (2001).
- <sup>29</sup>J. J. A. Baselmans, T. T. Heikkilä, B. J. van Wees, and T. M. Klapwijk, *Phys. Rev. Lett.* **89**, 207002 (2002).
- <sup>30</sup>J. J. A. Baselmans, B. J. van Wees, and T. M. Klapwijk, *Phys. Rev. B* **65**, 224513 (2002).
- <sup>31</sup>W. J. Skocpol, M. R. Beasley, and M. Tinkham, *J. Appl. Phys.* **45**, 4054 (1974).
- <sup>32</sup>H. Courtois, M. Meschke, J. T. Peltonen, and J. P. Pekola, *Phys. Rev. Lett.* **101**, 067002 (2008).
- <sup>33</sup>T. T. Heikkilä, J. Särkkä, and F. K. Wilhelm, *Phys. Rev. B* **66**, 184513 (2002).
- <sup>34</sup>A. D. Zaikin and G. F. Zharkov, *Sov. J. Low Temp. Phys.* **7**, 184 (1981).
- <sup>35</sup>J. C. Hammer, J. C. Cuevas, F. S. Bergeret, and W. Belzig, *Phys. Rev. B* **76**, 064514 (2007).
- <sup>36</sup>L. Angers, F. Chiodi, G. Montambaux, M. Ferrier, S. Guéron, H. Bouchiat, and J. C. Cuevas, *Phys. Rev. B* **77**, 165408 (2008).
- <sup>37</sup>V. T. Petrashov, V. N. Antonov, P. Delsing, and T. Claeson, *JETP Lett.* **60**, 606 (1994); available at [http://www.jetpletters.ac.ru/ps/1350/article\\_20401.shtml](http://www.jetpletters.ac.ru/ps/1350/article_20401.shtml).
- <sup>38</sup>W. Belzig, R. Shaikhaidarov, V. V. Petrashov, and Yu. V. Nazarov, *Phys. Rev. B* **66**, 220505 (2002).
- <sup>39</sup>M. Meschke, J. T. Peltonen, J. P. Pekola, and F. Giazotto, *Phys. Rev. B* **84**, 214514 (2011).
- <sup>40</sup>R. N. Jabdaraghi, M. Meschke, and J. P. Pekola, *Appl. Phys. Lett.* **104**, 082601 (2014).
- <sup>41</sup>A. Ronzani, C. Altimiras, and F. Giazotto, *Phys. Rev. Appl.* **2**, 024005 (2014).
- <sup>42</sup>F. Giazotto and F. Taddei, *Phys. Rev. B* **84**, 214502 (2011).
- <sup>43</sup>F. Zhou, P. Charlat, B. Spivak, and B. Pannetier, *J. Low Temp. Phys.* **110**, 841 (1998).
- <sup>44</sup>S. D'Ambrosio, M. Meissner, C. Blanc, A. Ronzani, and F. Giazotto, *Appl. Phys. Lett.* **107**, 113110 (2015).